Design, Synthesis and Pharmacological Characterization of a Fluorescent Agonist of the P2Y$_{14}$ Receptor

Evgeny Kiselev[a], Ramachandran Balasubramanian[a], Elisa Uliassi[a], Kyle A. Brown[b], Kevin Trujillo[a], Vsevolod Katritch[c], Eva Hammes[a], Raymond C. Stevens[c,d], T. Kendall Harden[b], and Kenneth A. Jacobson[a,*]

[a]Molecular Recognition Section, Laboratory of Bioorganic Chemistry, National Institute of Diabetes and Digestive and Kidney Diseases, National Institutes of Health, Bethesda, MD 20892, USA.

[b]Department of Pharmacology, University of North Carolina, School of Medicine, Chapel Hill, NC 27599, USA.

[c]The Bridge Institute, Department of Biological Sciences, Dornsife College of Letters, Arts and Sciences, University of Southern California, Los Angeles, CA 90089, USA.

[d]The Bridge Institute, Department of Chemistry, Dornsife College of Letters, Arts and Sciences, University of Southern California, Los Angeles, CA 90089, USA.

Abstract

The P2Y$_{14}$R is a G$_{i/o}$-coupled receptor of the P2Y family of purinergic receptors that is activated by extracellular UDP and UDP-glucose (UDPG). In an earlier report we described a P2Y$_{14}$R fluorescent probe, MRS4174, based on the potent and selective antagonist PPTN, a naphthoic acid derivative. Here, we report the design, preparation, and activity of an agonist-based fluorescent probe MRS4183 (**11**) and a shorter P2Y$_{14}$R agonist congener, which contain a UDP-glucuronic acid pharmacophore and BODIPY fluorophores conjugated through diaminoalkyl linkers. The design relied on both docking in a P2Y$_{14}$R homology model and established structure activity relationship (SAR) of nucleotide analogues. **11** retained P2Y$_{14}$R potency with EC$_{50}$ value of 0.96 nM (inhibition of adenylyl cyclase), compared to parent UDPG (EC$_{50}$ 47 nM) and served as a tracer for microscopy and flow cytometry, displaying minimal nonspecific binding. Binding saturation analysis gave an apparent binding constant for **11** in whole cells of 21.4±1.1 nM, with a t$_{1/2}$ of association at 50 nM **11** of 23.9 min. Known P2Y$_{14}$R agonists and PPTN inhibited cell binding of **11** with the expected rank order of potency. The success in the identification of a new P2Y$_{14}$R fluorescent agonist with low nonspecific binding illustrates the advantages of rational

*Address correspondence to: Laboratory of Bioorganic Chemistry, National Institute of Diabetes and Digestive and Kidney Diseases, NIH, Bethesda, MD 20892-0810 USA. Phone: 301-496-9024. Fax: 301-496-9024. kajacobs@helix.nih.gov. .

Supporting Information Available: Coordinate file of the P2Y$_{14}$R model-complex with **11**, synthetic procedures used for preparation of **10** and **11**, NMR and mass spectra of selected compounds and fluorescence spectra of **10** and **11**, are included.

design based on recently determined GPCR X-ray structures. Such conjugates will be useful tools in expanding the SAR of this receptor, which still lacks chemical diversity in its collective ligands.

Graphical abstract
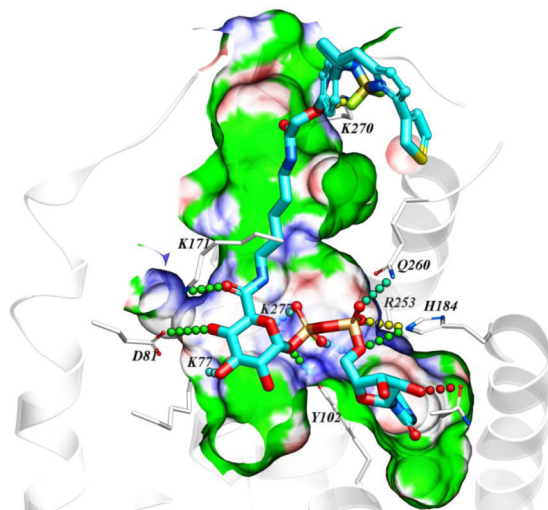
Keywords

G protein-coupled receptor; nucleotides; pyrimidines; homology modeling; docking; P2Y receptor

G protein-coupled receptors (GPCRs) that respond to extracellular uracil and adenine nucleotides (P2Y receptors, P2YRs) constitute important and ever-growing targets for pharmacological exploration. Eight nucleotide GPCRs are divided into two subfamilies of P2YRs, based on sequence and functional similarity: $P2Y_1R$-like, $P2Y_{1,2,4,6,11}$; and $P2Y_{12}R$-like, $P2Y_{12-14}$. The P2YRs are broadly distributed among many tissues and are expressed in immune cells, intestine, kidney, lung, nervous systems, and others.[1]

The $P2Y_{14}R$ is involved in inflammation, hypoxia[2] and mechanical pain hypersensitivity[3], and its activation enhances neutrophil chemotaxis[4] and promotes the release of mediators from mast cells.[5] Studies with $P2Y_{14}R^{-/-}$ mice suggested that $P2Y_{14}R$ antagonism might be a target for diabetes therapy; another study suggested that $P2Y_{14}R$ activation enhances insulin release.[6,19] Thus, the $P2Y_{14}R$ is a potential pharmaceutical target for inflammation, hypoxia, and endocrine mis-function.

Given the diversity of expression of the $P2Y_{14}R$ and the ubiquitous nature of its endogenous activators, i.e. UDP (Chart 1, **1**, EC_{50} 160 nM[20]) and UDP-sugars (**2**, EC_{50} 261 nM[8]; **4**, EC_{50} 370 nM[8]), the development of ligands selectively targeting this receptor is a considerable challenge and an important goal for pharmacological studies and potential therapeutic applications. A limited number of chemical classes have been identified as ligands and explored for their effects on the $P2Y_{14}R$: synthetic nucleotide analogues of **1** and **2**, such as **3** (EC_{50} 11 nM[20]),[7, 8] derivatives of 2-naphthoic acid, most notably the potent and selective antagonist 4-(4-(piperidin-4-yl)-phenyl)-7-(4-(trifluoromethyl)-phenyl)-2-

naphthoic acid (PPTN, **5**, K_B 0.43 nM),[9, 10, 11] and substituted pyrido[4,3-d]pyrimidines including potent analogue **6** (IC_{50} 10 nM).[12]

Nucleotide analogues of endogenous $P2Y_{14}R$ agonist **1** would be poor drug candidates due to their low bioavailability associated with high charge and their chemical instability due to hydrolysis by endonucleotidases. Derivatives of nonnucleotide $P2Y_{14}R$ antagonist **5** also suffer from poor drug-like characteristics due to high lipophilicity.[9, 13] However, the chemical stability, high affinity and selectivity of **5** toward the $P2Y_{14}R$ attracted our attention and inspired its use as a template for the development of fluorescent antagonist affinity probes.[10, 14] We applied virtual docking to design analogues of **5** that retain or enhance $P2Y_{14}R$ affinity and tolerate the increase in molecular size and interactions associated with fluorophore conjugation. A human (h) $P2Y_{14}R$ homology model was constructed based on the recently reported structures of the $hP2Y_{12}R$.[15, 16] This model was successfully utilized in predicting a suitable site on **5** for fluorophore conjugation and the minimum linker length required to provide adequate spacing between the pharmacophore and the fluorophore. The resulting PPTN-Alexa Fluor 488 conjugate (MRS4174, **7**) displayed sub-nanomolar antagonist affinity at the $hP2Y_{14}R$ and a very low level of nonspecific binding. Its binding to the $hP2Y_{14}R$ stably expressed in mammalian cells was inhibited by other $P2Y_{14}R$ ligands with the appropriate rank order of potency.

In the present study, we designed with the aid of molecular modeling and synthesized a pharmacologically complementary high affinity fluorescent agonist-based probe. The suitability of the site of attachment and the dependence of potency on the length of the spacer chain were predicted by a structure-based analysis using a homology model of the $P2Y_{14}R$.[14,21] Our previous modeling study concluded that the glucose moiety of **4** was the most structurally permissive region of this endogenous agonist since it bound in the second subpocket of the $P2Y_{14}R$ binding site, which is accessible to the extracellular medium. Therefore, two fluorescent derivatives of **4** were designed and prepared (Scheme 1) based on predictions from computational modeling of $P2Y_{14}R$ agonist binding.[21] The strategy behind the selection of these target compounds is described below. The conjugation of a fluorophore was accomplished via condensation of commercially available fluorescent amines with the carboxylic group of **4**.

Based on previous structure activity relationship (SAR) studies of **2**, two designs of fluorescent affinity probes of varying chain length were compared. The structures of **1** and **2**, now identified as endogenous $P2Y_{14}R$ agonists, have been extensively probed by chemical modification with regard to their ability to activate the $P2Y_{14}R$, as well as $P2Y_2$, $P2Y_4$ and $P2Y_6Rs$.[7, 8, 17]. The C6 carbon of the hexose moiety of UDPGA **4** was found suitable for chain extension with retention of $P2Y_{14}R$ agonist activity. A number of amide derivatives at the glucose C6 have been constructed, and most of these derivatives retained agonist activity. It was also found that $P2Y_{14}R$ agonist activity was retained with attachment of large groups such as unprotected, as well as acetyl- and Boc-protected aminoethylamides, and polyamidoamine (PAMAM) dendrimers of generation (G) 3 and 6 attached to the C6 carbon.[17] Moreover, it was found that dendrimer conjugates possessed enhanced potency when compared to **4**.

Thus, we chose the structure of **4** as a starting point for designing and building fluorescent probes. Our objectives were to facilitate the availability of such affinity probes and to validate further the previously constructed computational models. Hence, we chose as our primary fluorophore boron-dipyrromethene (BODIPY), which has been used in other fluorescent probes of GPCRs.[18] Unlike the chemical series of hydrophobic P2Y$_{14}$R antagonist **5**, in which a less hydrophobic fluorophore, AlexaFluor 488, in conjugate **7** was optimal, the restriction of choosing a hydrophilic fluorophore was relieved due to the inherent high polarity and hydrophilicity of **4**. Additionally, various BODIPY dyes with built-in reactive amine linkers of varying length are readily available commercially. Two amide-bound conjugates, **10** and MRS4183 **11** (Scheme 1), were docked into a homology model of the hP2Y$_{14}$R to predict their fit prior to synthesis. The target molecules **10** and **11** contained linkers consisting of 7 and 14 (including benzene ring) atoms, respectively, between C6 of hexose and the pyrrole ring of BODIPY.

A homology model of the hP2Y$_{14}$R was constructed as we reported, based on the high resolution X-ray crystallographic structure of the P2Y$_{12}$R complex with 2-MeSADP.[15, 16, 21] Various known P2Y$_{14}$R agonists were docked in the orthosteric binding site. The attempted docking of the fluorescent agonists **10** and **11** did not provide a satisfactory binding pose for conjugate **10**, suggesting the inability of the binding pocket to accommodate both pharmacophore and fluorophore connected by a short, 7-atom linker containing ethylene diamine. However, the hypothetical binding mode of **11** revealed that the longer, 14-atom linker containing 1,5-diaminopentane is sufficiently long to connect the pharmacophore inside the deep binding site with the fluorophore presented on the extracellular side of the receptor (Figure 1). According to the obtained binding mode, the nucleobase binds inside the pocket formed by TMs 3–5, including aromatic stacking with Y102$^{3.33}$ (using standard numbering relative to the TMs[26]) and with carbonyl oxygen atoms forming hydrogen bond contacts with side chains of H184$^{5.35}$ and N188$^{5.39}$. The ribose hydroxyls form contacts with N156$^{4.57}$ side chain and the backbone carbonyl of C94$^{3.25}$. The diphosphate moiety forms salt bridges with positively charged K77$^{2.60}$, K277$^{7.35}$, and R253$^{6.55}$, and makes polar contacts with Y102$^{3.33}$ and Q260$^{6.60}$ side chains. The amide functionalities of the linker were found to form hydrogen bond contacts with the side chain of K171 (EL2) on the interior of the receptor and the backbone of K270 (EL3) on the extracellular part. The linker projects toward the extracellular region via a channel along TM3 and through the window formed by EL1 and EL2.

The synthesis of derivatives **10** and **11** was accomplished using standard coupling conditions involving the primary amine congeners of the dyes (**8** and **9**) and the carboxylate group of UDP-glucuronic acid **4**. In particular, **10** was synthesized initially using 1-[bis(dimethylamino)methylene]-1H-1,2,3-triazolo[4,5-b]pyridinium 3-oxid hexafluorophosphate (HATU) as coupling agent and NEt$_3$ as a base, while in the case of **11** different conditions were tried (Table S1, Supporting Information) to increase the reaction yield and simplify the purification process. Indeed, the first attempt (condition A) to synthetize **11** resulted in an impure product even after several successive purification attempts, due to an impurity co-eluting with the desired product. The higher reactivity of a different coupling agent, [[(Z)-(1-cyano-2-ethoxy-2-oxoethylidene)amino]oxy-morpholin-4-

ylmethylidene]-dimethylazanium hexafluorophosphate (COMU, conditions B and C), compared to HATU led to the formation of numerous side products during the reaction that complicated the purification process (2 or 3 purifications) without leading to a significant detectable amount of title compound. Nevertheless, the best performing procedure (condition D), using excess **4** (1.5 equivalents), COMU (1.5 equivalents) as coupling agent and DIPEA (2 equivalents) as base, provided the desired, pure product after one purification step using a C18 HPLC column, however, in a very low yield (0.3%). **11** was found to have excitation and emission maxima at 590 and 616 nm, respectively (Figure S2, Supporting information).

Both **10** and **11** were evaluated functionally in Chinese hamster ovary (CHO) cells stably expressing the Gi-coupled human P2Y$_{14}$R (CHO- P2Y$_{14}$R) for capacity to inhibit forskolin-stimulated 3′,5′-cyclic adenosine monophosphate (cAMP) accumulation (Figure 2).[10] UDPGABODIPY conjugate **11** retained its agonist activity with a nanomolar EC$_{50}$ value. The EC$_{50}$ value of 0.96 nM for inhibition of cAMP production in hP2Y$_{14}$R-expressing CHO cells, compared to 47 nM for **4**, constitutes a 50-fold potency enhancement in the fluorescent conjugate. Thus, **11** improved upon the potency of parent UDP-sugars despite the presence of a large fluorophore attached to its hexose C6 position. Accordingly, **11** demonstrated strong specific binding to P2Y$_{14}$R-CHO cells in flow cytometry (FCM) (Figures 3A, B & C). The level of nonspecific binding determined by coincubating with up to 200 nM **5** was very low. We also quantified saturation of binding of **11** to CHO cells expressing P2Y$_{14}$R using FCM. Increasing concentrations of **11** from 1 nM to 500 nM were used to calculate the total binding, and nonspecific binding was determined in the presence of 20 μM **5**. From the saturation curve, an apparent binding constant (Kd app) was determined to be 21.4±1.1 nM (Figure 4A). The kinetics of **11** binding in CHO cells expressing P2Y$_{14}$R was studied using FCM, and the t$_{1/2}$ of binding of 50 nM **11** was 23.9 min (Figure 4B).

Competition for fluorescent binding with known P2Y$_{14}$R ligands and P2Y$_6$R ligands was also performed. These two types of ligands were compared because both receptors are activated by UDP, and no other P2YRs respond to UDP. To determine the K$_i$ values of known ligands, we used **11** as a tracer, at a concentration of 50 nM. Competitive binding results with known nucleotide agonists and nonnucleotide antagonist **5** shown in Table 1 roughly followed the expected rank order of P2Y$_{14}$R potency (**5** >> **3** > **1** > **2** > **4**). The P2Y$_6$R agonist MRS2957 **12**, a dinucleoside triphosphate, also inhibited binding of **11**, but with a K$_i$ value of 5.18 μM, which is about 500-fold higher than its EC$_{50}$ value (12 nM) for activation of the P2Y$_6$R.[24] The nonnucleotide antagonist of P2Y$_6$R, MRS2578 **13**,[25] did not show any significant binding to P2Y$_{14}$R at 10 μM, thus confirming its P2Y$_6$R selectivity. As predicted by computational modeling, conjugate **10** was much weaker than **11**, with an EC$_{50}$ of 91 nM for inhibition of cAMP accumulation in P2Y$_{14}$R-CHO cells. However, over a range of concentrations (0.05 −1 μM) it did not demonstrate significant fluorescence binding in comparison to nonspecific binding in FCM experiments (data not shown).

Confocal fluorescence microscopy indicated specific labeling of P2Y$_{14}$R-CHO cells by **11** (Figure 5). The fluorescent labeling was inhibited in the presence of competing antagonist **5** and was also absent in control CHO cells lacking P2Y$_{14}$R expression (not shown). The label appears irregularly distributed on the surface of the cells and partially internalized,

consistent with **11** being an agonist of the P2Y$_{14}$R. Similarly, the internalization of fluorescent agonists of other P2YRs and GPCRs was reported.[22,23]

In conclusion, we applied computational tools and known P2Y$_{14}$R agonist SAR toward design of a new agonist fluorescent probe. An insensitive site on the glucose moiety of **4** was covalently derivatized, and two linkers of different length were tested both computationally and experimentally. The demonstrated predictive strength of the utilized approach highlights the validity and usefulness of this particular P2Y$_{14}$R homology model and the strategy at large when applied toward probe design. Additionally, the lack of fluorescent binding of the analogue **10** with a shorter linker and the strong binding of **11** provide an additional estimate of the shape, size and depth of the orthosteric ligand binding pocket of the P2Y$_{14}$R. Thus, we have used insights from P2YR structures and modeling to identify **11** as a useful agonist fluorescent probe of the P2Y$_{14}$R, which has high affinity and low nonspecific binding. Its binding properties and inhibition by known P2YR ligands could readily be determined using FCM. Our previous efforts to characterize this receptor included the design and preparation of a fluorescent probe based on the potent and selective antagonist **5**. In order to further the study the role and distribution of this receptor, we introduce here a useful fluorescent probe that is pharmacologically complementary to our reported nonnucleotide fluorescent antagonist **7**. The utility of this probe to detect P2Y$_{14}$R using fluorescence microscopy was also demonstrated. Further studies with regard to fluorescence binding of both agonist and antagonist probes and receptor pharmacology as well as their suitability for ligand affinity screening are currently underway.

Supplementary Material

Refer to Web version on PubMed Central for supplementary material.

Acknowledgments

List of abbreviations

BODIPY	boron-dipyrromethene
cAMP	3′,5′-cyclic adenosine monophosphate
CHO	Chinese hamster ovary
COMU	[[(Z)-(1-cyano-2-ethoxy-2-oxoethylidene)amino]oxy-morpholin-4-ylmethylidene]-dimethylazanium hexafluorophosphate
DMEM	Dulbecco's modified Eagle's medium
DMF	dimethylformamide
ECL	extracellular loop

FCM	flow cytometry
HATU	1-[bis(dimethylamino)methylene]-1H-1,2,3-triazolo[4,5-b]pyridinium 3-oxid hexafluorophosphate
IBMX	3-isobutyl-1-methylxanthine
2-MeSADP	2-methylthioadenosine-5′-diphosphate
MESF	molecules of equivalent soluble fluorochrome
MRS2578	*N*,*N*''-1,4-butanediyl*bis*[*N*'-(3-isothiocyanatophenyl)]thiourea]
MRS2957	P^1-(uridine 5′-)-P^3-(N^4-methoxycytidine 5′-)triphosphate
PPTN	4-(4-(piperidin-4-yl)-phenyl)-7-(4-(trifluoromethyl)-phenyl)-2-naphthoic acid
SAR	structure activity relationship
UDPG	uridine-5′-diphosphoglucose
TM	transmembrane helix

References

1. Boeynaems J-M, Communi D, Robaye B. Wiley Interdisciplinary Reviews: Membrane Transport and Signaling. 2012; 1:581.

2. Lazarowski ER, Harden TK. Mol. Pharmacol. 2015; 88:151. [PubMed: 25829059]

3. Kobayashi K, Yamanaka H, Yanamoto F, Okubo M, Noguchi K. Glia. 2012; 60:1529. [PubMed: 22736439]

4. Sesma JI, Kreda SM, Steinckwich-Besancon N, Dang H, Garcia-Mata R, Harden TK, Lazarowski ER. A. J. Physiol. Cell Physiol. 2012; 303:C490.

5. Gao ZG, Ding Y, Jacobson KA. Biochem. Pharmacol. 2010; 79:873. [PubMed: 19896471]

6. Xu J, Morinaga H, Oh D, Li P, Chen A, Talukdar S, Mamane Y, Mancini JA, Nawrocki AR, Lazarowski E, Olefsky JM, Kim JJ. J. Immunol. 2012; 189:1992. [PubMed: 22778393]

7. Ko H, Fricks I, Ivanov AA, Harden TK, Jacobson KA. J. Med. Chem. 2007; 50:2030. [PubMed: 17407275]

8. Ko H, Das A, Carter RL, Fricks IP, Zhou Y, Ivanov AA, Melman A, Joshi BV, Kovac P, Hajduch J, Kirk KL, Harden TK, Jacobson KA. Bioorg. Med. Chem. 2009; 17:5298. [PubMed: 19502066]

9. Gauthier JY, Belley M, Deschenes D, Fournier JF, Gagne S, Gareau Y, Hamel M, Henault M, Hyjazie H, Kargman S, Lavallee G, Levesque JF, Li L, Mamane Y, Mancini J, Morin N, Mulrooney E, Robichaud J, Therien M, Tranmer G, Wang Z, Wu J, Black WC. Bioorg. Med. Chem. Lett. 2011; 21:2836. [PubMed: 21507640]

10. Barrett MO, Sesma JI, Ball CB, Jayasekara PS, Jacobson KA, Lazarowski ER, Harden TK. Mol. Pharmacol. 2013; 84:41. [PubMed: 23592514]

11. Belley, M.; Deschenes, D.; Fortin, R.; Fournier, JF.; Gagne, S.; Gareau, Y.; Gauthier, JY.; Li, L.; Robichaud, J.; Therien, M. Patent. 2009.

12. Guay D, Beaulieu C, Belley M, Crane SN, DeLuca J, Gareau Y, Hamel M, Henault M, Hyjazie H, Kargman S, Chan CC, Xu L, Gordon R, Li L, Mamane Y, Morin N, Mancini J, Therien M, Tranmer G, Truong VL, Wang Z, Black WC. Bioorg. Med. Chem. Lett. 2011; 21:2832. [PubMed: 21507642]

13. Robichaud J, Fournier JF, Gagne S, Gauthier JY, Hamel M, Han Y, Henault M, Kargman S, Levesque JF, Mamane Y, Mancini J, Morin N, Mulrooney E, Wu J, Black WC. Bioorg. Med. Chem. Lett. 2011; 21:4366. [PubMed: 21689930]

14. Kiselev E, Barrett MO, Katritch V, Paoletta S, Weitzer CD, Brown KA, Hammes E, Yin AL, Zhao Q, Stevens RC, Harden TK, Jacobson KA. ACS Chem. Biol. 2014; 9:2833. [PubMed: 25299434]

15. Zhang J, Zhang K, Gao ZG, Paoletta S, Zhang D, Han GW, Li T, Ma L, Zhang W, Müller CE, Yang H, Jiang H, Cherezov V, Katritch V, Jacobson KA, Stevens RC, Wu B, Zhao Q. Nature. 2014; 509:119. [PubMed: 24784220]

16. Zhang K, Zhang J, Gao ZG, Zhang D, Zhu L, Han GW, Moss SM, Paoletta S, Kiselev E, Lu W, Fenalti G, Zhang W, Müller CE, Yang H, Jiang H, Cherezov V, Katritch V, Jacobson KA, Stevens RC, Wu B, Zhao Q. Nature. 2014; 509:115. [PubMed: 24670650]

17. Das A, Zhou Y, Ivanov AA, Carter RL, Harden TK, Jacobson KA. Bioconjugate Chem. 2009; 20:1650.

18. Vernall AJ, Hill SJ, Kellam B. Br. J. Pharmacol. 2014; 171:1073. [PubMed: 23734587]

19. Meister J, Le Duc D, Ricken A, Burkhardt R, Thiery J, Pfannkuche H, Polte T, Grosse J, Schöneberg T, Schulz A. J. Biol. Chem. 2014; 289:23353. [PubMed: 24993824]

20. Das A, Ko H, Burianek LE, Barrett MO, Harden TK, Jacobson KA. J. Med. Chem. 2010; 53:471. [PubMed: 19902968]

21. Trujillo K, Paoletta S, Kiselev E, Jacobson KA. Bioorg. Med. Chem. 2015; 23:4056. [PubMed: 25868749]

22. Jayasekara PS, Barrett MO, Ball CB, Brown KA, Kozma E, Costanzi S, Squarcialupi L, Balasubramanian R, Maruoka H, Jacobson KA. Med. Chem. Comm. 2013; 4:1156.

23. Jayasekara PS, Barrett MO, Ball CB, Brown KA, Hammes E, Balasubramanian R, Harden TK, Jacobson KA. J. Med. Chem. 2014; 57:3874. [PubMed: 24712832]

24. Maruoka H, Barrett MO, Ko H, Tosh DK, Melman A, Burianek LE, Balasubramanian R, Berk B, Costanzi S, Harden TK, Jacobson KA. J. Med. Chem. 2010; 53:4488. [PubMed: 20446735]

25. Mamedova L, Joshi BV, Gao ZG, von Kügelgen I, Jacobson KA. Biochem. Pharmacol. 2004; 67:1763. [PubMed: 15081875]

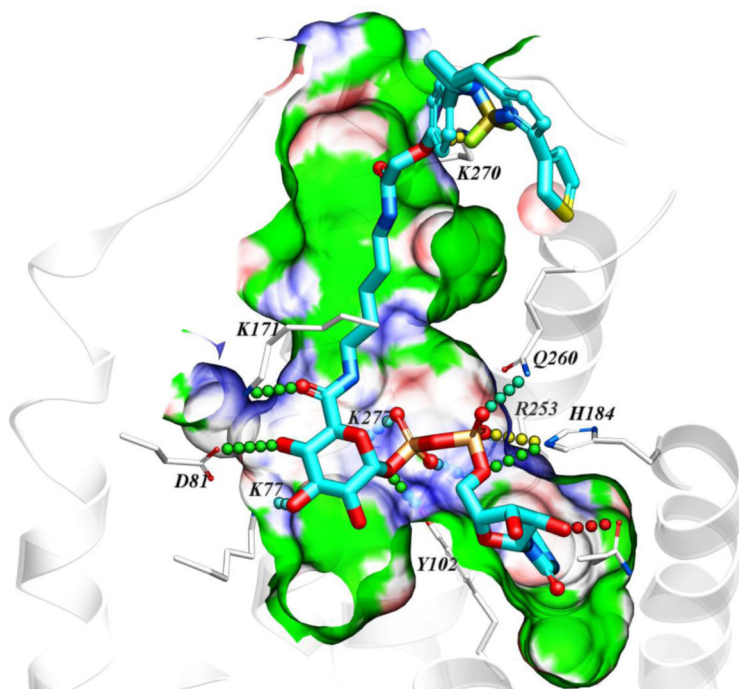26. Ballesteros JA, Weinstein H. Methods Neurosci. 1995; 25:366.

Figure 1.
Hypothetical binding mode of **11** in a hP2Y$_{14}$R homology model based on the structure of the nucleotide-bound hP2Y$_{12}$R.[14,21] 12 The BODIPY fluorophore is predicted to interact with residues of the ELs, including K270. Other residues shown correspond to TMs: 2 (K77$^{2.60}$, D81$^{2.64}$); 3 (Y102$^{3.33}$); 5 (H184$^{5.35}$, N188$^{5.39}$); 6 (R253$^{6.55}$, Q260$^{6.62}$); 7 (K277$^{7.35}$).
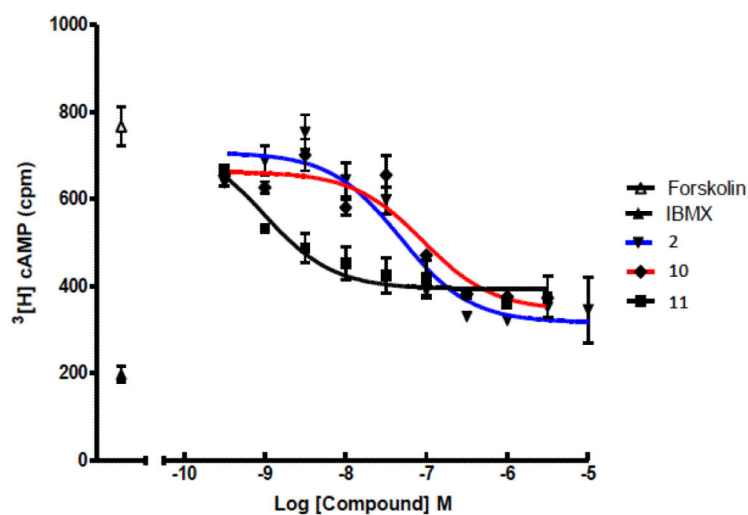
Figure 2.
Concentration-response curves for endogenous agonist **2** (blue), short-chain conjugate **10** (red) and long-chain conjugate **11** (black) for inhibition of forskolin-stimulated cAMP formation in P2Y$_{14}$R-expressing CHO cells, as described.[14] Incubations were at 37 °C for 15 min and were terminated by aspiration of medium and addition of 500 μL of ice-cold 5% trichloroacetic acid. All assays with **6**, **22**, and **30** also contained 30 μM forskolin and 200 μM IBMX, 3-isobutyl-1-methylxanthine, a phosphodiesterase inhibitor. Data points for IBMX alone (indicated by IBMX in the legend) and forskolin + IBMX (indicated by forskolin in the legend) also are shown.
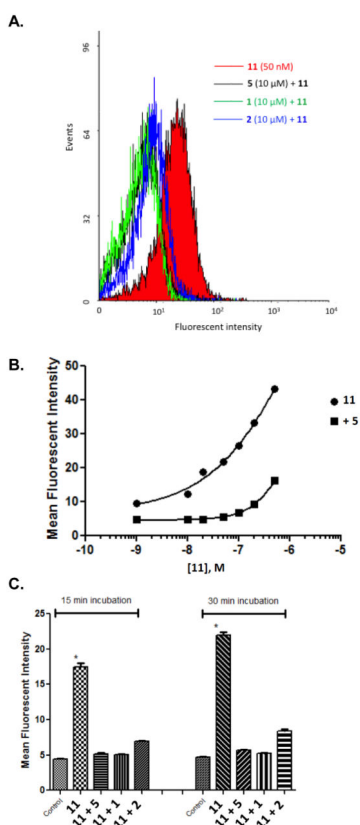
Figure 3.
(A) Inhibition of binding of **11** in P2Y$_{14}$R-CHO cells by antagonist PPTN **5** and agonists UDP **1** and UDPG **2** (10 μM), analyzed by flow cytometry. Incubation of cells for 30 min with antagonist **5** or agonist **1** or **2** (all at 10 μM) followed by incubation with **11** (50 nM) for 30 min was performed. (B) Dependence of fluorescent labeling of P2Y$_{14}$R-CHO cells on the concentration of **11**, analyzed by flow cytometry. Incubation of cells with a variable concentration of **11** (1 nM – 500 nM) was performed following 60 min of incubation in the absence or presence of PPTN 5 (200 nM). Nearly complete inhibition of binding was observed up to 100 nM **11**. (C) Fluorescence ligand binding experiments using FCM in P2Y$_{14}$R-CHO cells with **11** (50 nM) after 30 min pre-incubation at 37 °C with known P2Y$_{14}$R agonists **1** and **2** or P2Y$_{14}$R antagonist **5** (each 10 μM). Each column shows the fluorescent intensity of each compound using **11** normalized to 100% for each time point and after correcting the mean fluorescence intensity values for auto fluorescence. Results are expressed as mean±S.E (n=3).
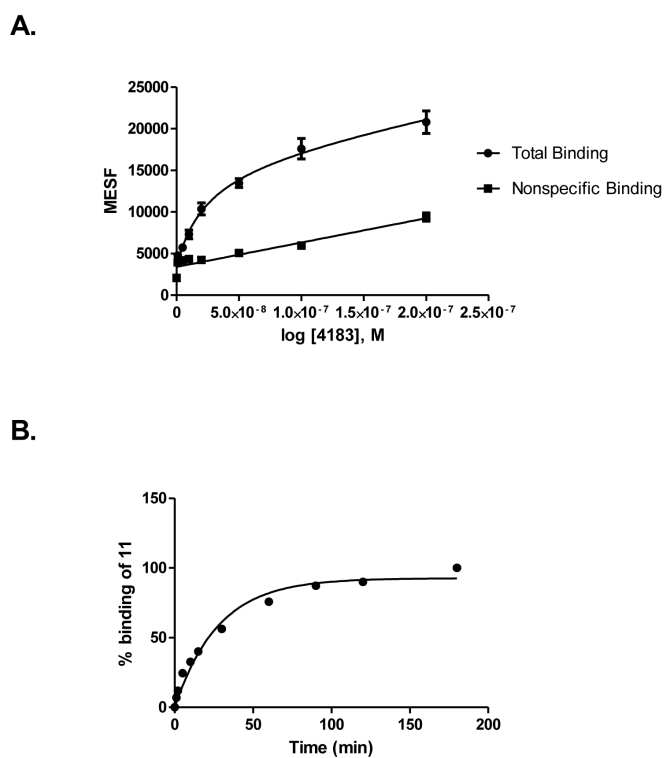
A.

B.

Figure 4.
(A) Saturation binding assays (B) binding kinetics with tracer **11** using FCM following incubation for 30 min with CHO cells expressing the hP2Y$_{14}$R. Mean fluorescent Intensity values from FCM were converted to MESF values (Figure S6) using Quickcal program v. 2.3 (Bangs Laboratories Inc., Fishers, IN). Nonspecific binding was measured in the presence of **11** and 20 μM **5**. Results are expressed as mean±S.E (n=3). In (A), the Kd value is 26.1±3.6 nM, Bmax = 44,400 MESF (n=3). In (B), 100% corresponds to a MESF value of 26,900.

Figure 5.
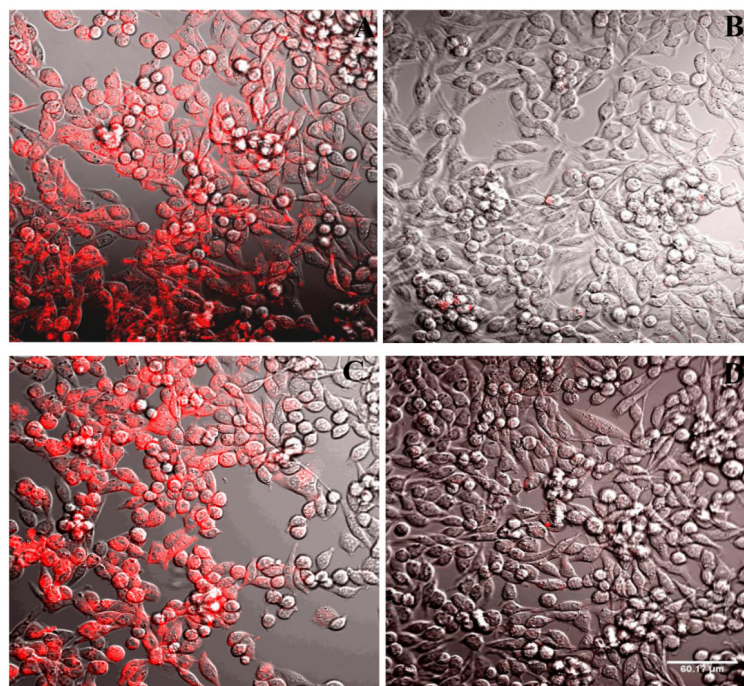Fluorescence confocal microscopy. Fluorescent labeling of P2Y$_{14}$R-CHO cells by **11**, analyzed by confocal fluorescence microscopy. Incubation of cells with a fixed concentration of **11** (200 nM) was performed following 30 min (A, B) or 120 min (C, D) of incubation in the absence (A, C) or presence (B, D) of antagonist **5** (10 μM). The complete inhibition of binding was observed in the presence of the antagonist. Scale of 60 μm is shown in D. The excitation laser used had a peak at 555 nm and was equipped with a 561 nm filter. Emitted fluorescence was measured without a filter.
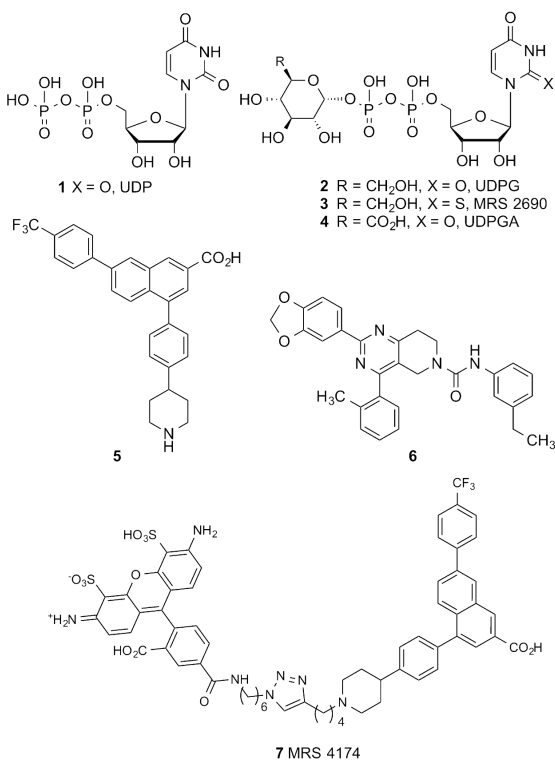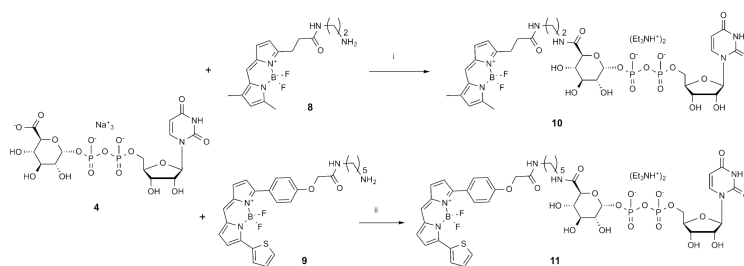
Chart 1.
Representative P2Y$_{14}$R agonists **1**–**4**, antagonists **5**, **6** and fluorescent antagonist MRS 4174 **7**.

Scheme 1.
Synthesis of fluorescent conjugates of **4**. [a]Reagents and conditions: i: HATU, Et$_3$N, DMF, 23 °C, 2% yield; ii: COMU (1.5 eq.), DIPEA (2 eq.), DMF, 0 °C, 0.3% yield.

Table 1

Inhibition of P2Y$_{14}$R binding in whole cells by known ligands of P2Y$_{14}$R and P2Y$_6$R using **11** as a FCM tracer. Results are expressed as mean±S.E (n=3).[a]

Compound	hP2Y$_{14}$R cAMP assay (EC$_{50}$ or IC$_{50}$[b], μM)	FCM binding at hP2Y$_{14}$R (K$_i$, μM)
P2Y$_{14}$ ligands		
1 UDP	0.160	0.63±0.03
2 UDP-glucose	0.261	2.23±0.2
3 MRS2690	0.011	0.34±0.04
4 UDP-glucuronic acid	0.370	5.3±0.4
5 PPTN	0.00043	0.0019±0.0001
P2Y$_6$ ligands		
12 MRS2957[c]	ND	5.18±0.20
13 MRS2578[c]	ND	No inhibition at 10 μM

[a]FCM binding was measured in CHO cells expressing the hP2Y$_{14}$R using a fixed concentration (50 nM) of **11**, following an incubation of 30 min. Values in the cAMP assay were from published reports.[10,20,21,24] ND, not determined.

[b]IC$_{50}$ values for P2YR antagonists **5** and **13**.

[c]Structures: